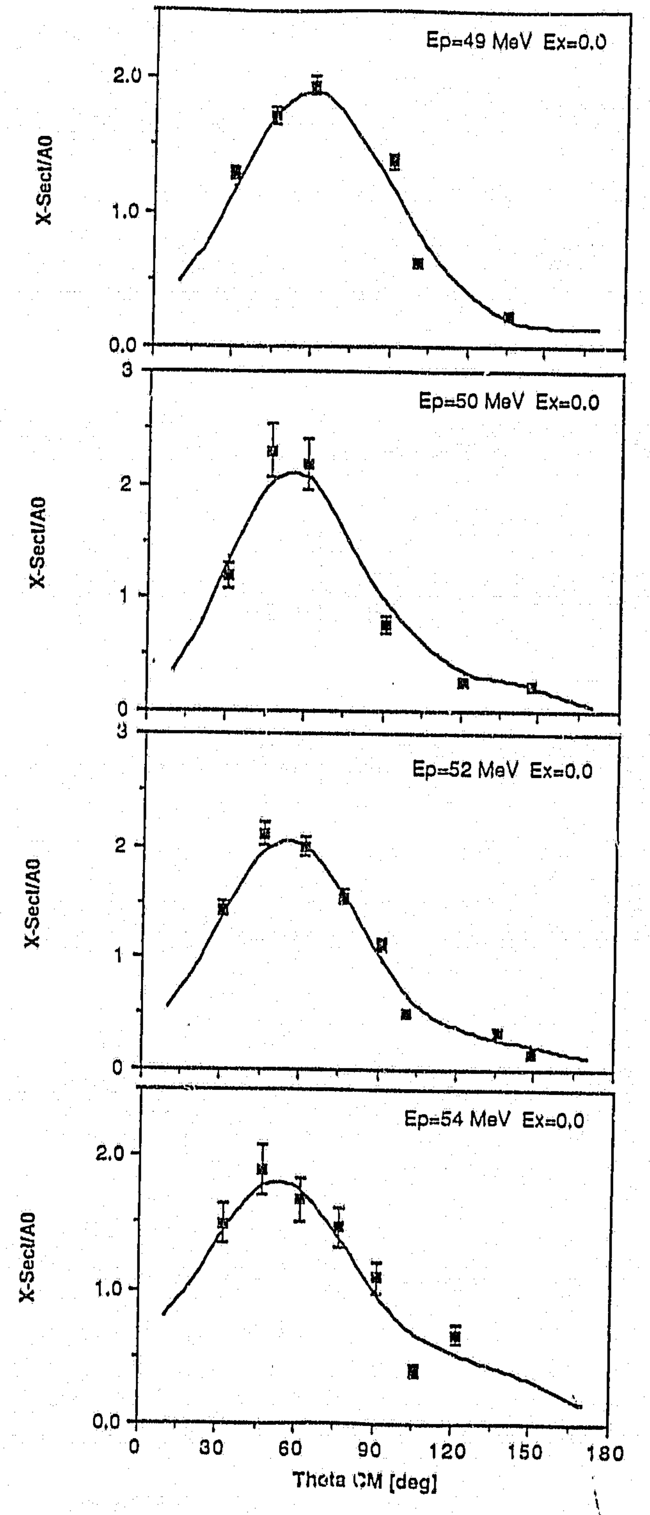

FIGURE 10 Angular distributions for the reaction $^{12}C(p,\gamma_x)^{13}N^*[E_x = 0.0\,\text{MeV}]$ at E_p from 49 to 54 MeV. The full curves are Legendre polynomial fits to the experimental points.

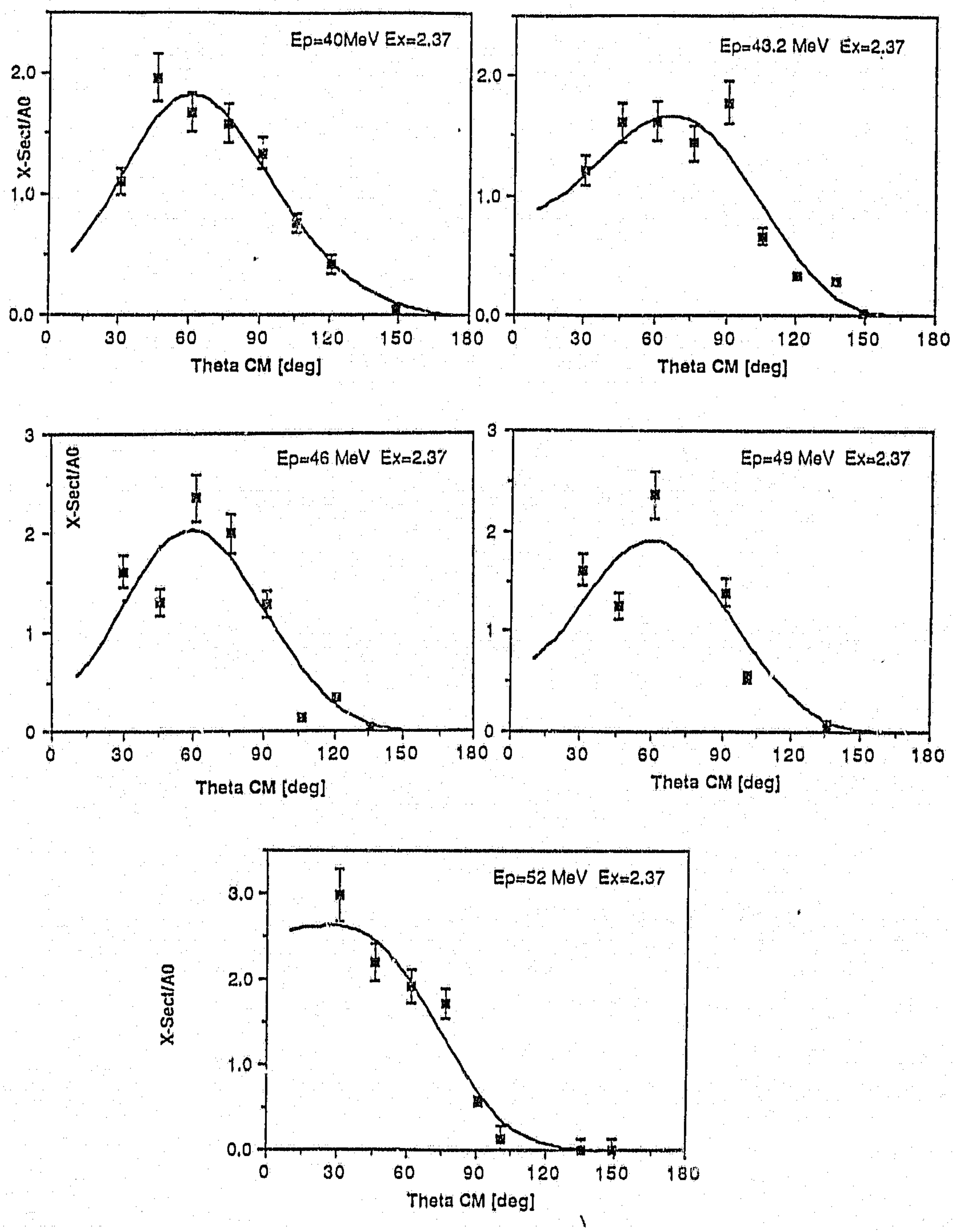

FIGURE 11 Angular distributions for the reaction $^{12}C(p,\gamma_x)^{13}N^*[E_x = 2.37\,\mathrm{MeV}]$ at E_p from 40 to 52 MeV. The full curves are Legendre polynomial fits to the experimental points.

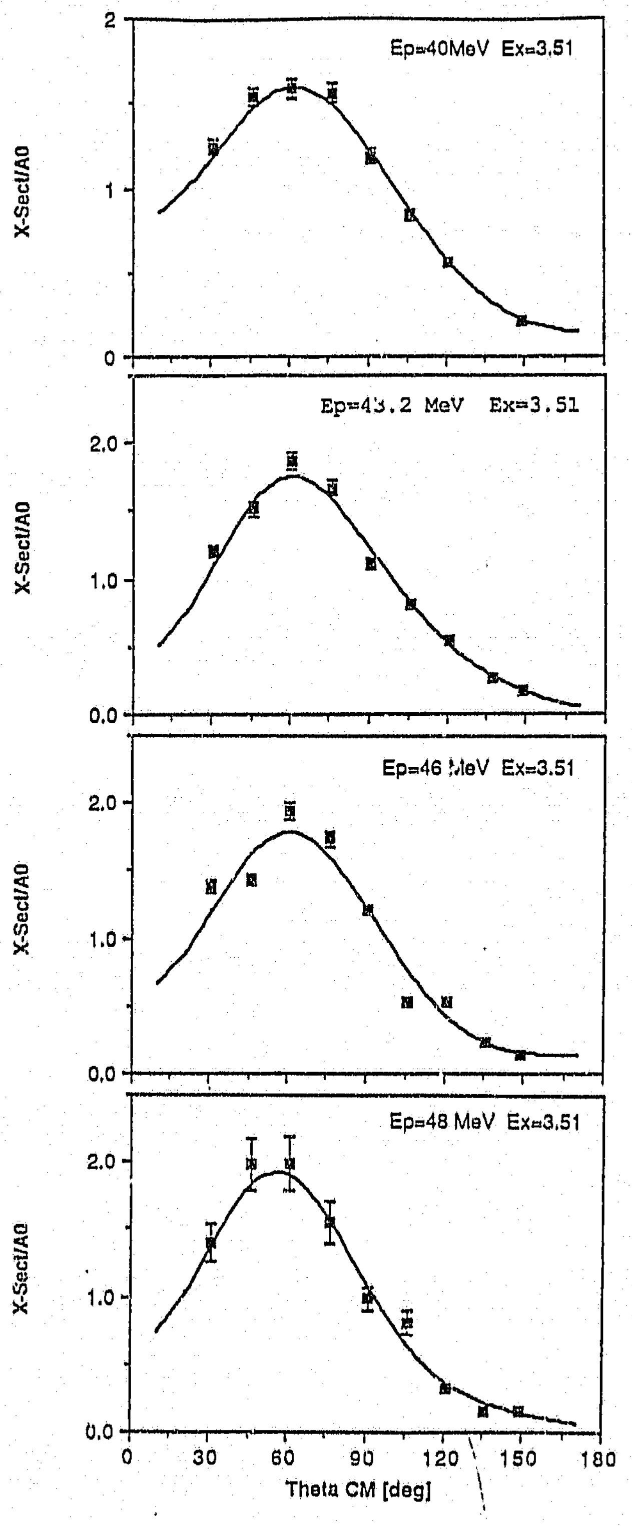

FIGURE 12 Angular distributions for the reaction $^{12}C(p,\gamma_{\pi})^{13}N^{*}[E_x = 3.51\,MeV]$ at E_p from 40 to 48 MeV. The full curves are Legendre polynomial fits to the experimental points.

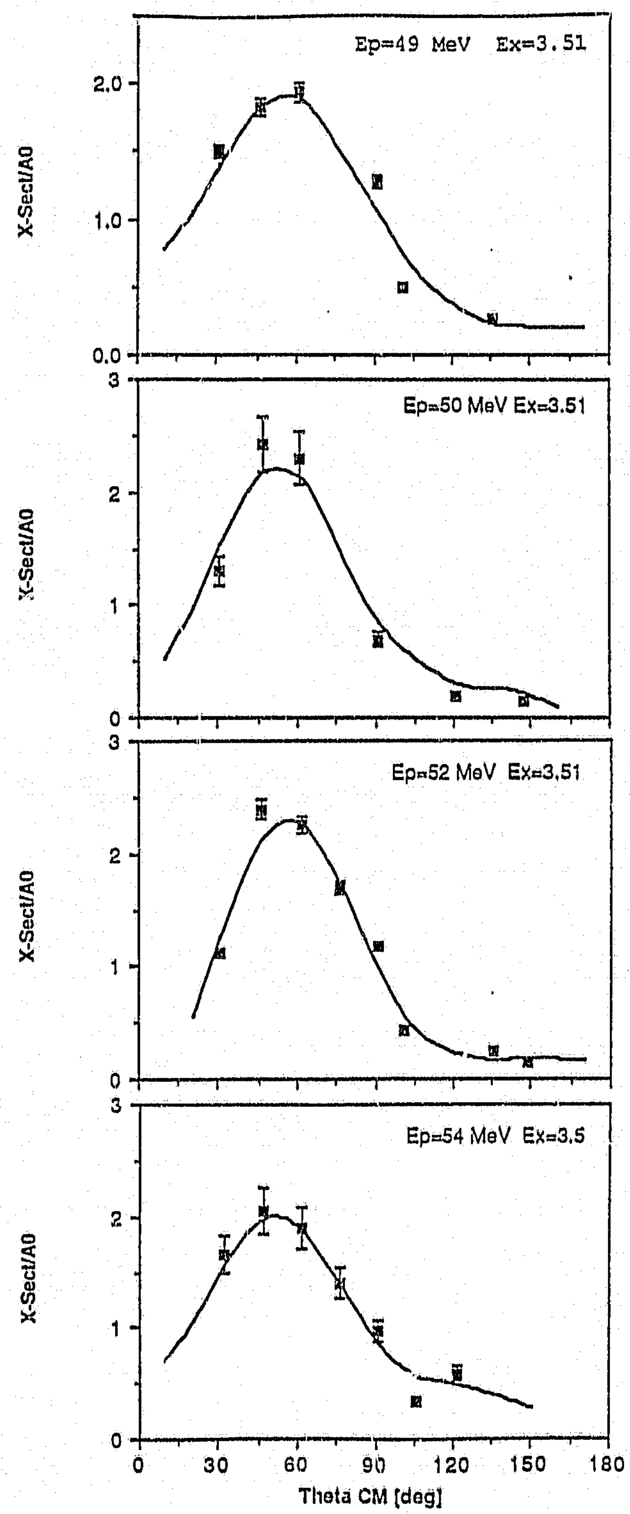

FIGURE 13 Angular distributions for the reaction $^{12}C(p,\gamma_x)^{13}N^*[E_x = 3.51\,MeV]$ at E_p from 49 to 54 MeV. The full curves are Legendre polynomial fits to the experimental points.

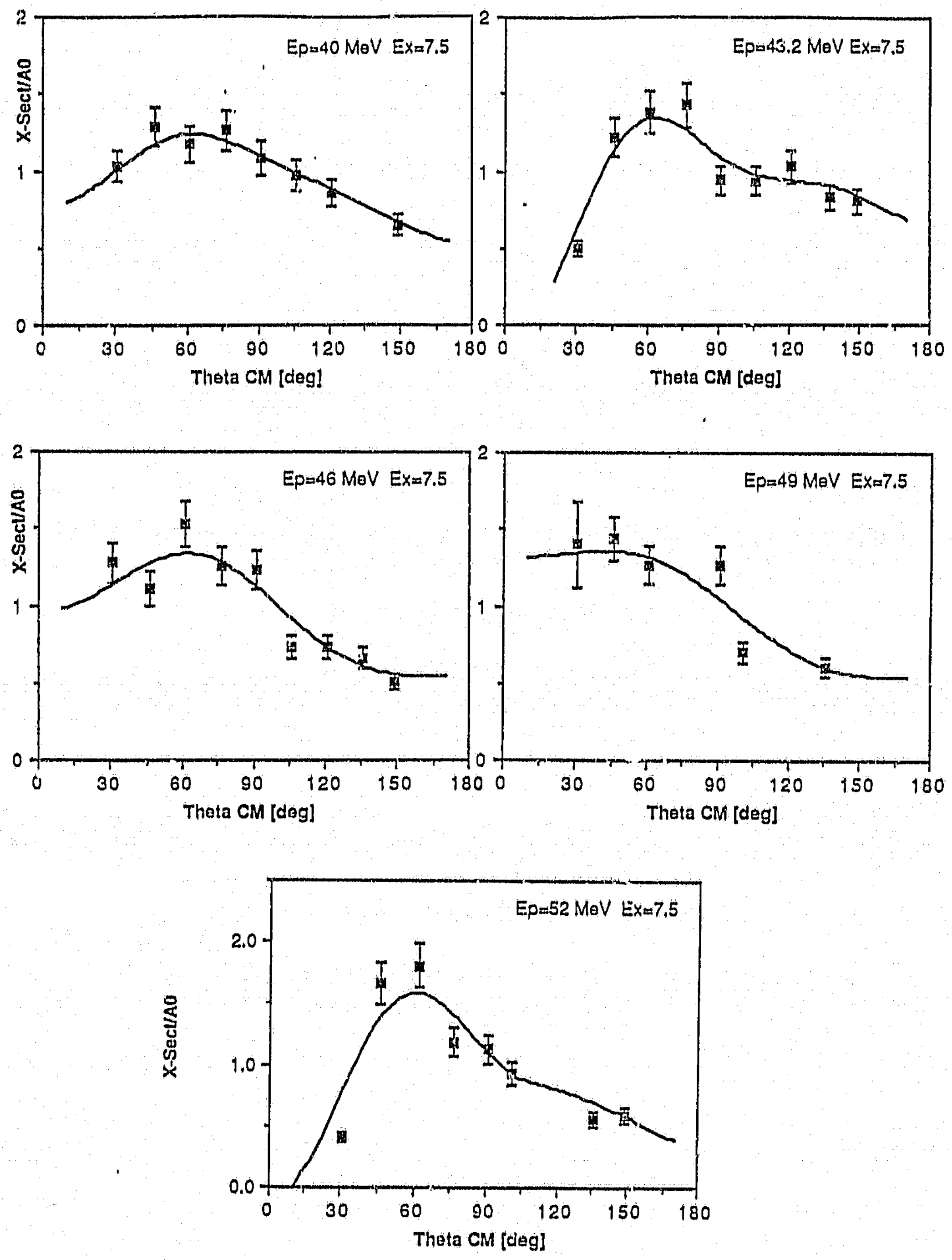

FIGURE 14 Angular distributions for the reaction $^{12}C(p,\gamma_x)^{13}N^*[E_x = 7.5\,\text{MeV}]$ at E_p from 40 to 52 MeV. The full curves are Legendre polynomial fits to the experimental points.

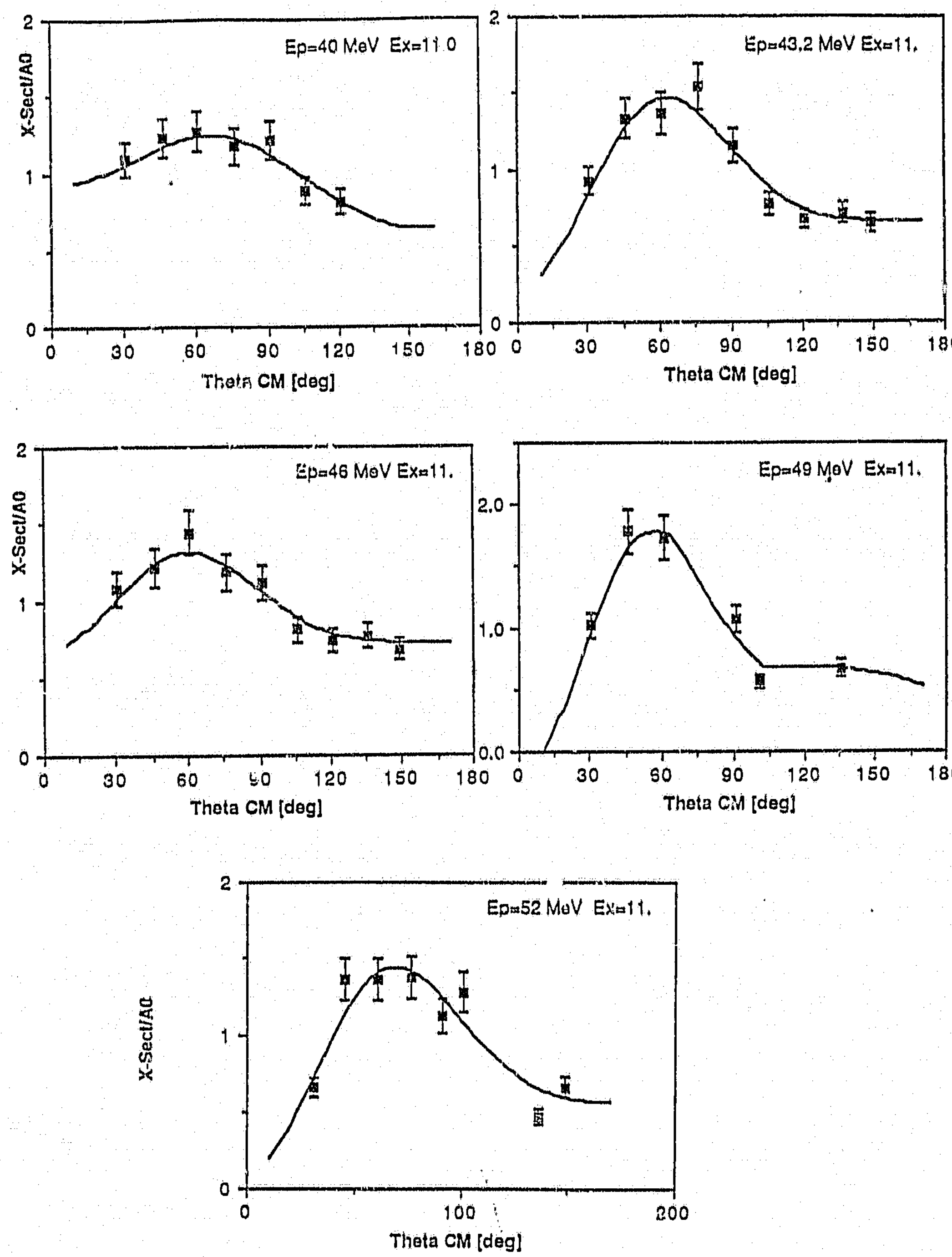

FIGURE 15 Angular distributions for the reaction $^{12}C(p,\gamma_x)^{13}N^*[E_x = 11.\,MeV]$ at E_p from 40 to 52 MeV. The full curves are Legendre polynomial fits to the experimental points.

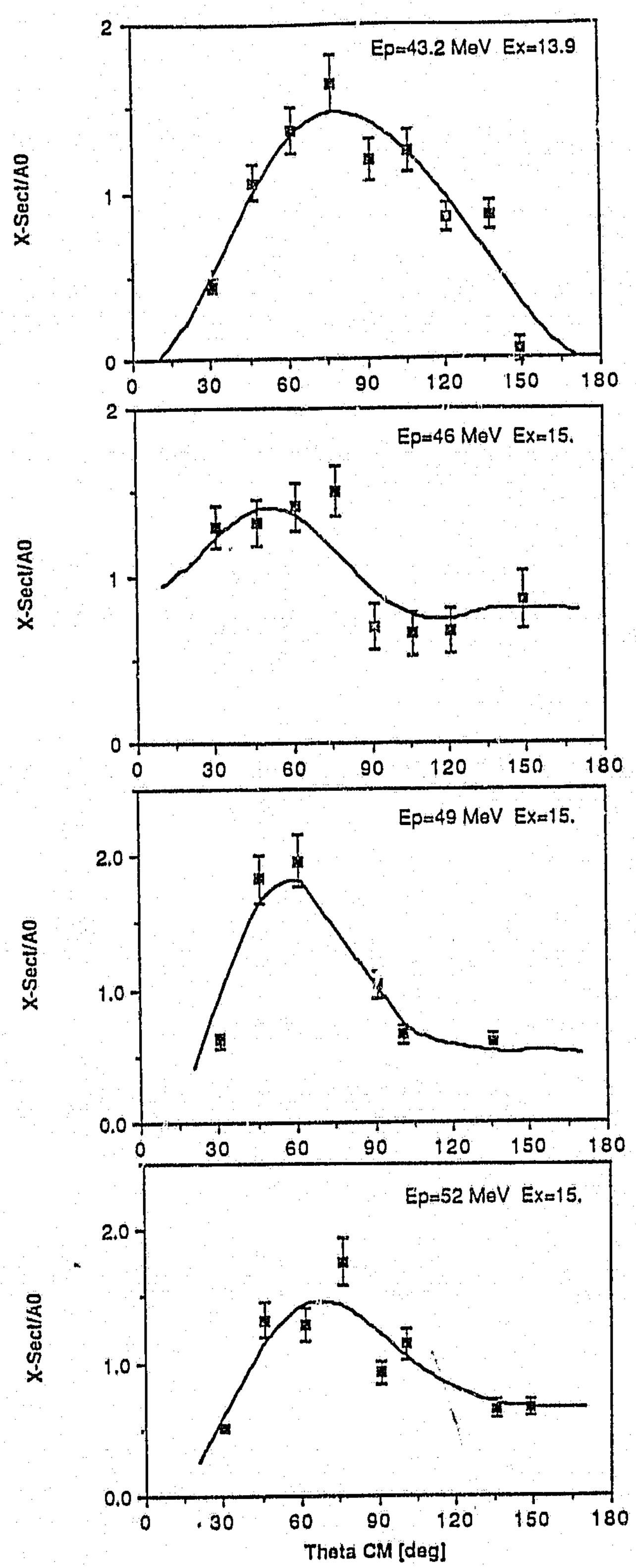

FIGURE 16 Angular distributions for the reaction $^{12}C(p,\gamma_x)^{13}N^*[E_x = 15.\,MeV]$ at E_p from 40 to 52 MeV. The full curves are Legendre polynomial fits to the experimental points.

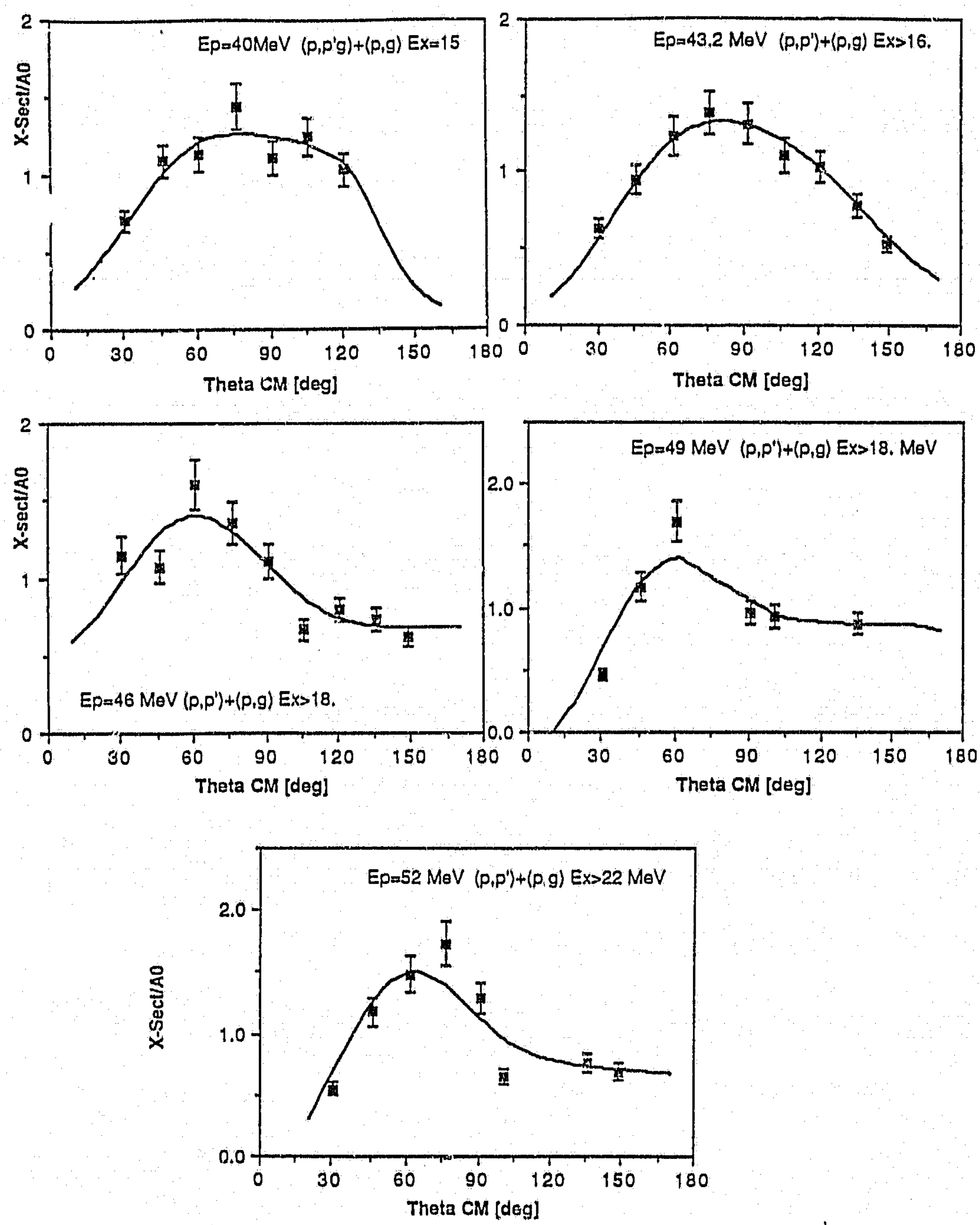

FIGURE 17 Angular distributions for the reaction $^{12}C(p,p'\gamma)^{12}C^*$ superimposed on competing $^{12}C(p,\gamma_x)^{13}N^*$ transitions at E_p from 40 to 52 MeV. The full curves are Legendre polynomial fits to the experimental points.

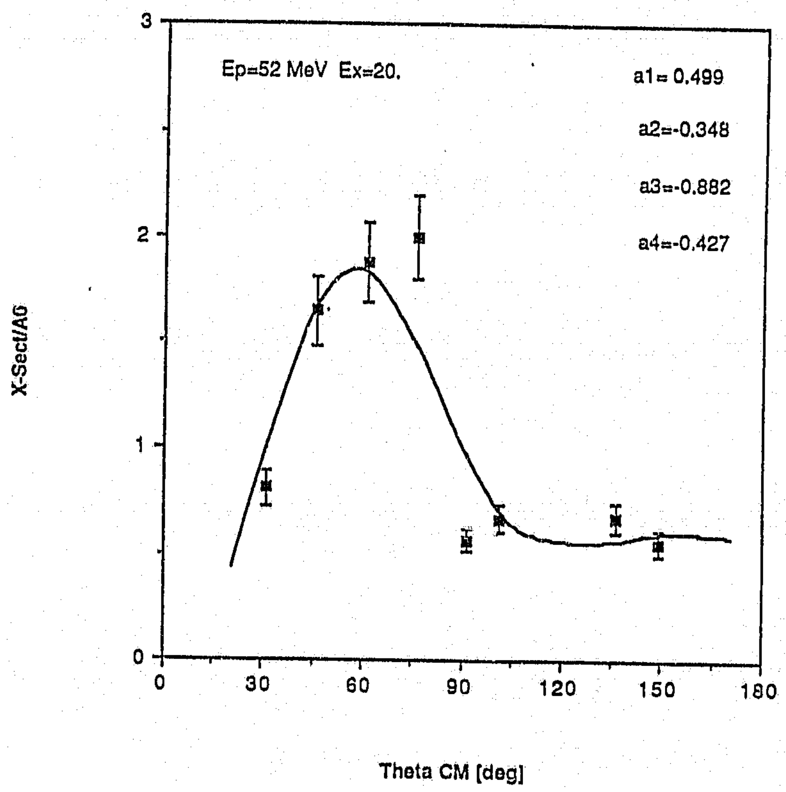

FIGURE 18 Angular distribution for the reaction $^{12}C(p,\gamma_x)^{13}N^*[E_x = 20.\,MeV]$ at $E_p = 52\,MeV$. The full curve is a Legendre polynomial fit to the experimental points. The relative a_l coefficients are also reported.

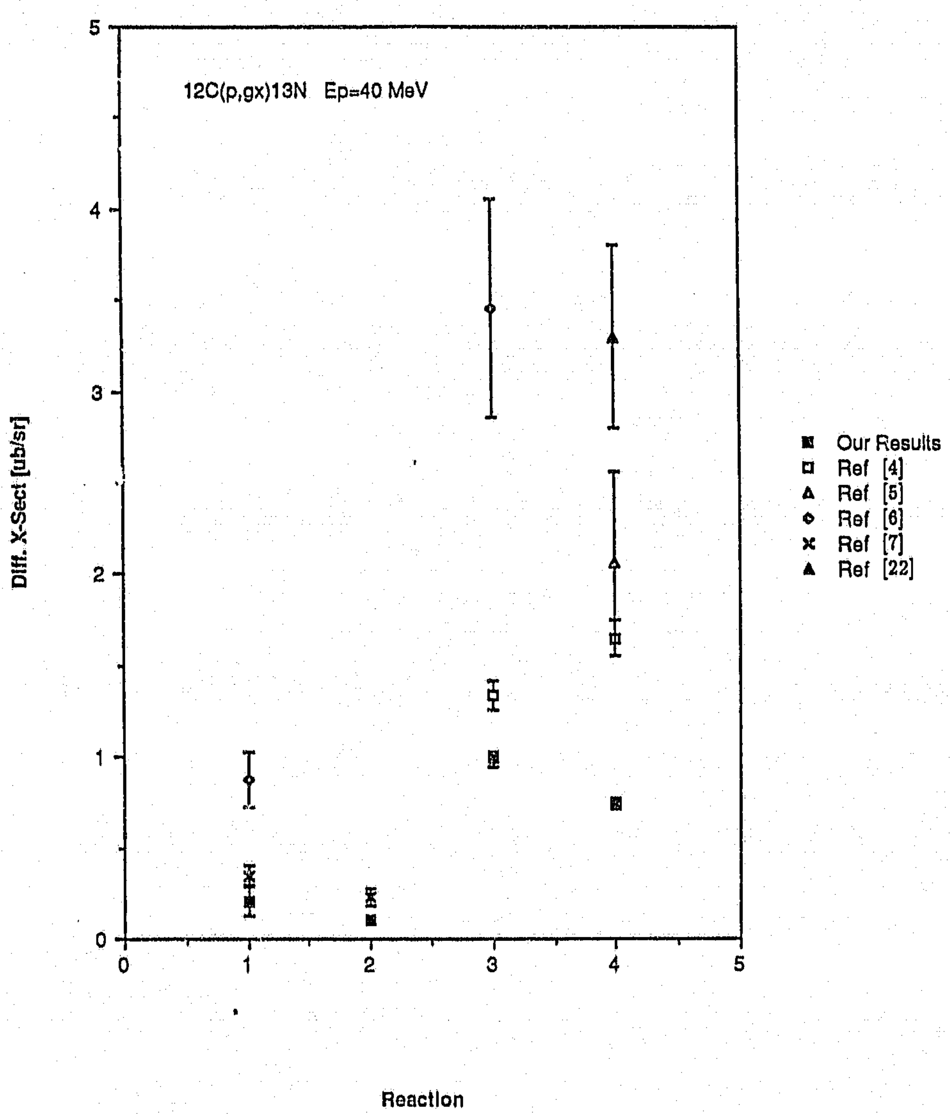

FIGURE 19 A comparison of (p,γ) cross sections extracted from different experiments to show the large discrepancies of existent data. The X-axis is used to mark different reaction channels. Reaction 1 is the (p,γ_0) at 60 deg; reaction 2 is the (p,γ_1) at 60 deg; reaction 3 is the (p,γ_{2+3}) at 60 deg and reaction 4 is the (p,γ_{2+3}) at 90 deg.

any other for all compared exit channels, including the prominent γ_0 and γ_{2+3} ones that should, in principle, be affected by the lowest statistical uncertainties. Our points differ from the closest ones, including errors, by about 25% except for the (γ_{2+3}) point at 90 deg were the discrepancy is by a factor of 2. We would once more like to emphasize *a)* the completeness of our experiment that covers in this energy range a large number of runs and experimental points per run so to guarantee a very low probability of repeated large systematic errors, and *b)* our meticulous fitting procedure which should lead to lower cross sections since more background is subtracted. We proceed now to a detailed analysis of our results.

From the angular distributions of figures 9-18 it is evident that the measurement of 9 points per energy allows the assessment of fine details even at the extreme excitation energies explored. All (p,γ) distributions show remarkable similarities. For any projectile energy and final level excitation energy the angular distributions peak systematically between 60 deg and 70 deg. In detail we can observe the individual behaviour of the a_i coefficients in figures 20 to 26. It is more appropriate to compare the energy behaviour of a given coefficient for any of the final ^{13}N excited states involved as done in figure 27, where for convenience of reading the error bars have been removed. It is evident from the consideration of all data, that the most accurate sets concern the ground and the second exited state transitions, the other angular distributions being affected at times by evident distortions, that could be ascribed to untraced systematic errors, and that will certainly introduce uncertainties in the interpretation of data.

Let us first focus attention on the (p,γ_0) and the the (p,γ_{2+3}) channels alone recalling how angular coefficients are related to the possible multipolarities (Table 5). It is sensible to include in our considerations the E1, E2 and eventually E3 amplitudes. Magnetic multipolarities are strongly reduced with respect to the electric ones and only M1 has been considered in previous analyses: but the M1 strength is found to decrease rapidily with energy and the contribution of the (E1,M1) interference term to the a_1 coefficient should therefore be negligible in our case compared to the effect of the (E1,E2) interference. For the other Legendre polynomial coefficients M1 contributes only to higher order terms (see table 5). It was demonstrated by a group (including the author [4]) for ^{12}C and ^{16}O

TABLE 5

Multipole dependence of angular distribution Legendre coefficients

a_n b_n	1^{st} ord kR	2^{nd} ord kR	3^{rd} ord kR	4^{th} ord kR	5^{th} ord kR
a_0	$\|E1\|^2$		$\|E2\|^2 + \|M1\|^2$		$\|E3\|^2 + \|M2\|^2$
a_1 b_1		$(E1, E2)$		$(E2, E3)$	
		$(E1, M1)$		$(E2, M2)$	
				$(M1, M2)$	
a_2 b_2	$\|E1\|^2$		$\|E2\|^2$		$\|E3\|^2$
	$(E1, E1')$		$\|M1\|^2$		$(E3, E3')$
			$(E1, E3)$		$\|M2\|^2$
			$(E1, M2)$		$(M2, M2')$
			$(M1, E2)$		$(E3, M2)$
			$(E2, E2')$		
			$(M1, M1')$		
a_3 b_3		$(E1, E2)$		$(E2, E3)$	
				$(E2, M2)$	
				$(M1, M2)$	
				$(M1, E3)$	
a_4 b_4			$\|E2\|^2$		$\|E3\|^2$
			$(E1, E3)$		$(E3, E3')$
			$(E2, E2')$		$\|M2\|^2$
					$(M2, M2')$
					$(E3, M2)$
a_5 b_5				$(E2, E3)$	
a_6 b_6					$\|E3\|^2$
					$(E3, E3')$

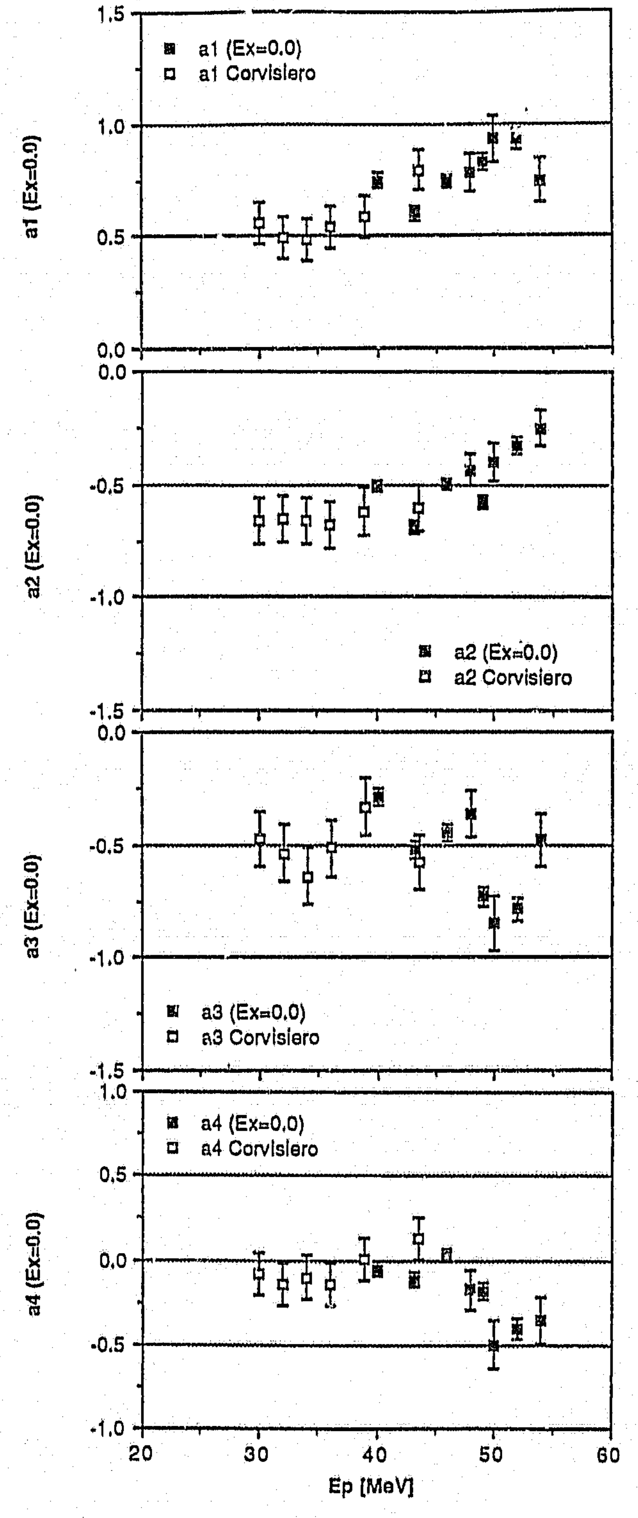

FIGURE 20 Legendre polynomial coefficients as a function of proton energy for the reaction $^{12}C(p,\gamma_x)^{13}N^*$ at $[E_x = 0.0\,\mathrm{MeV}]$. The open squares are data from reference [4], the full square are the results of this work.

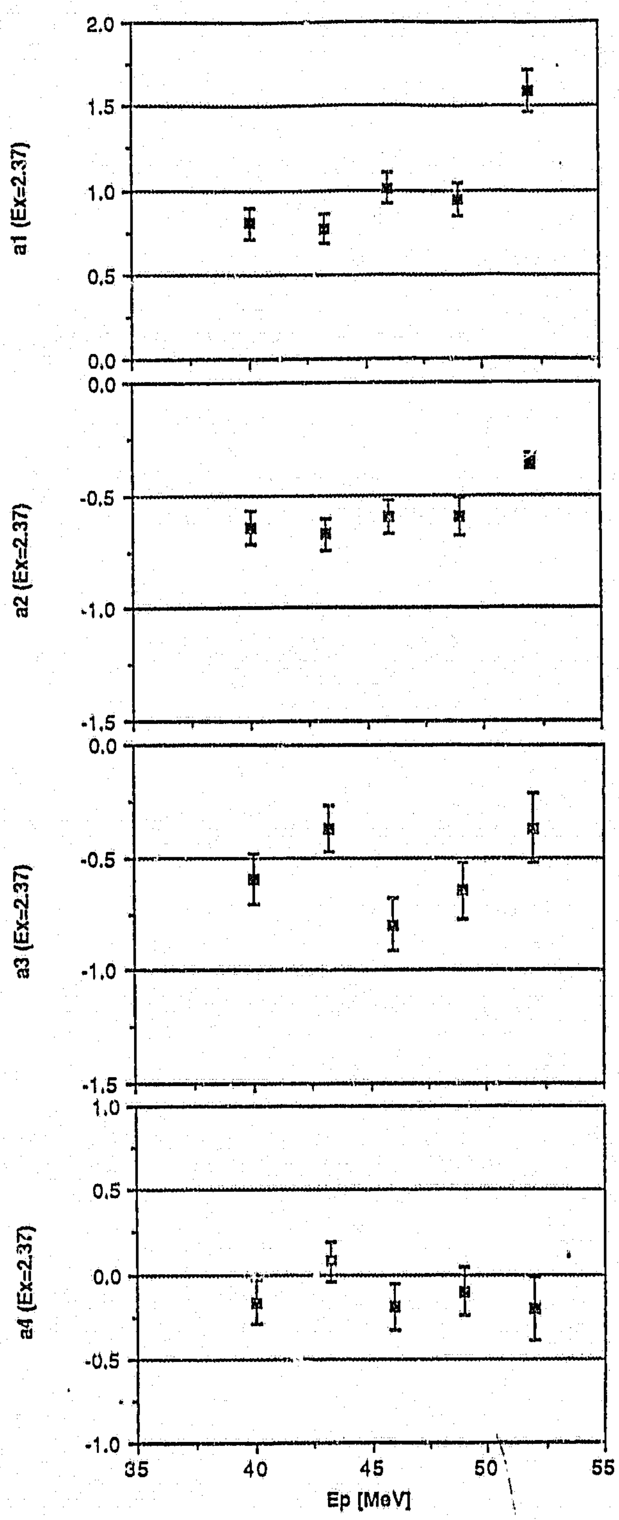

FIGURE 21 Legendre polynomial coefficients as a function of proton energy for the reaction $^{12}C(p,\gamma_u)^{13}N^*$ at $[E_x = 02.37\,\text{MeV}]$.

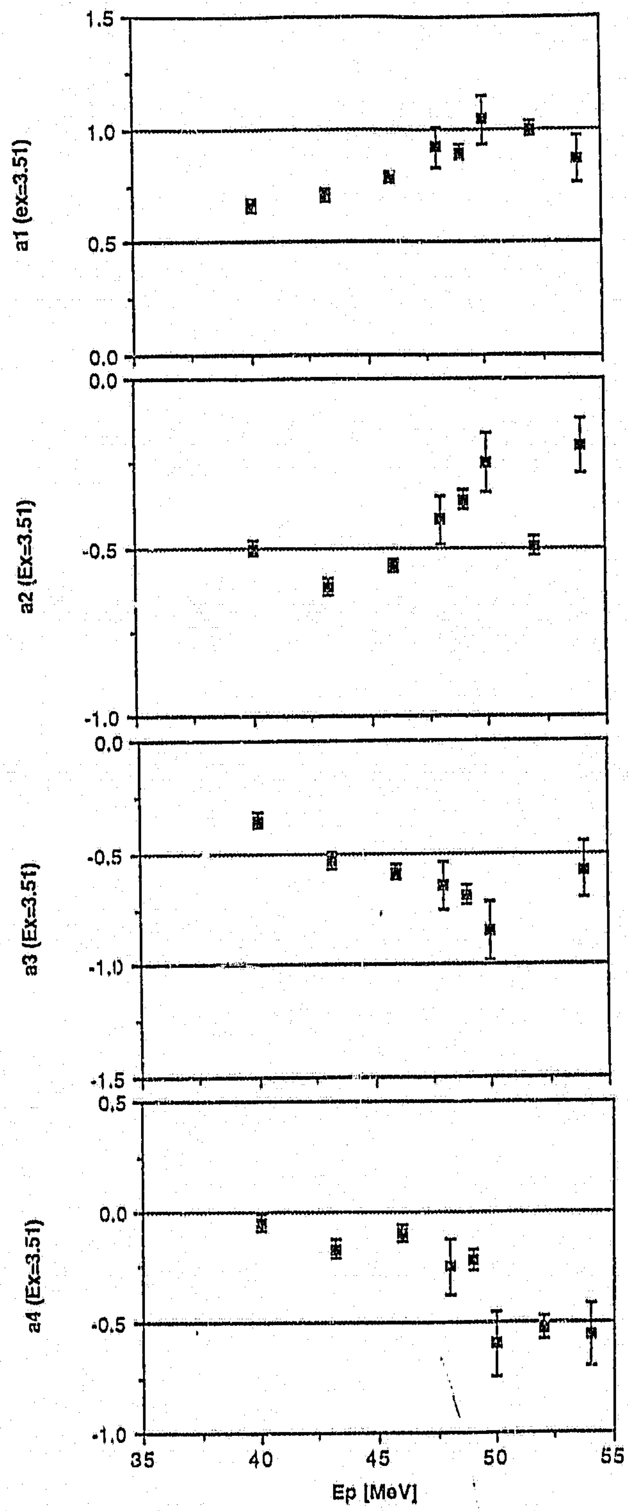

FIGURE 22 Legendre polynomial coefficients as a function of proton energy for the reaction $^{12}C(p,\gamma_x)^{13}N^*$ at $[E_x = 3.51\,\text{MeV}]$.

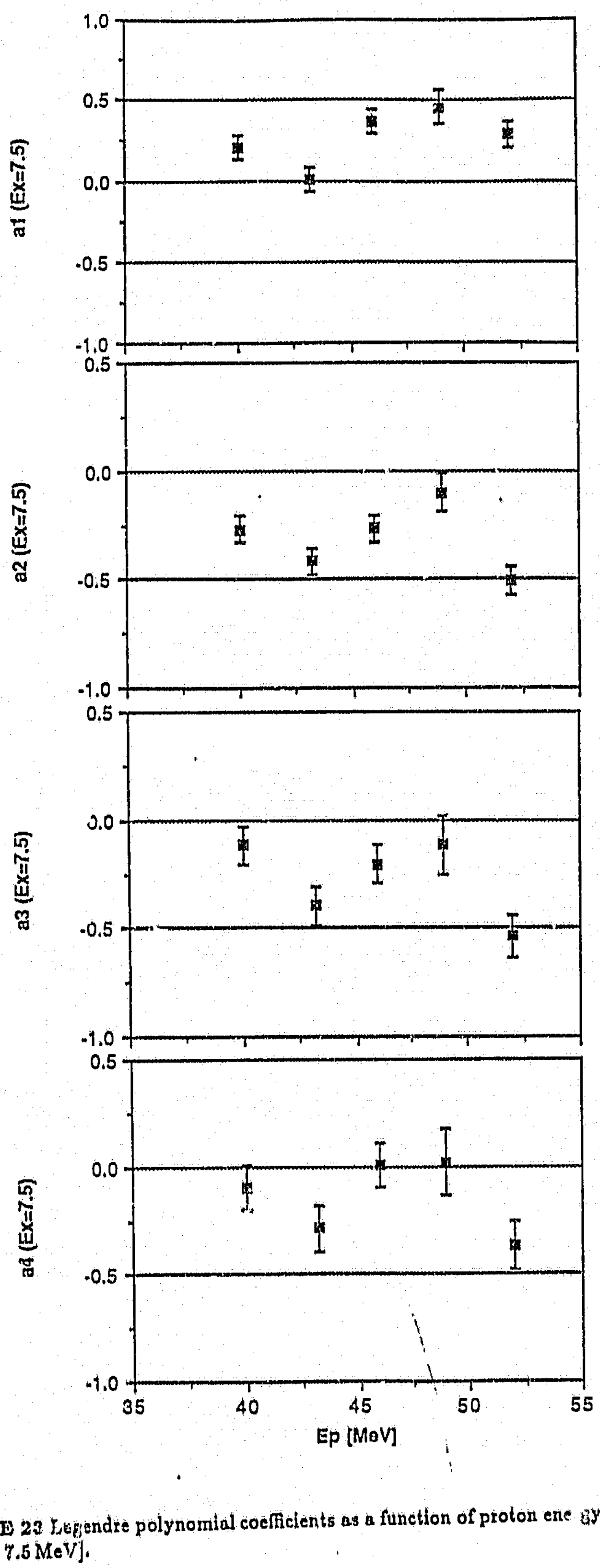

FIGURE 23 Legendre polynomial coefficients as a function of proton energy for the reaction $^{12}C(p,\gamma_x)^{13}N^*$ at $[E_x = 7.5\,\mathrm{MeV}]$.

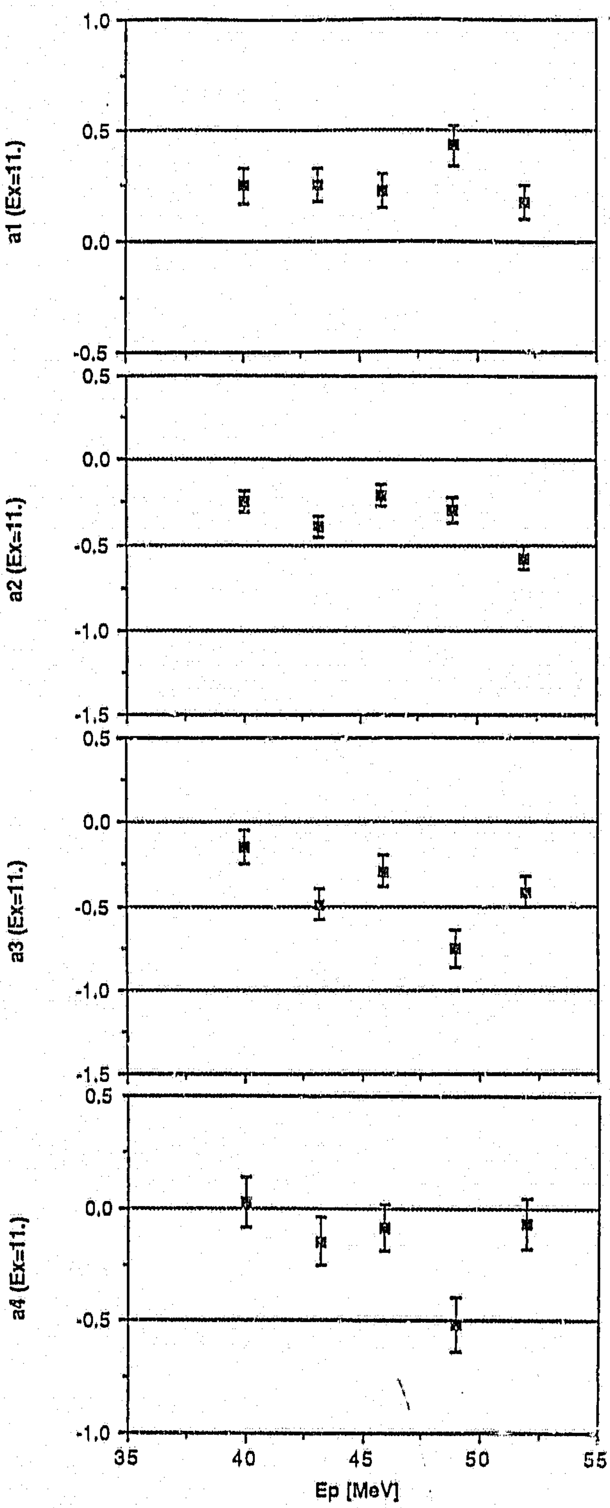

FIGURE 24 Legendre polynomial coefficients as a function of proton energy for the reaction $^{12}C(p,\gamma_x)^{13}N^*$ at $[E_x = 11.\ \mathrm{MeV}]$.

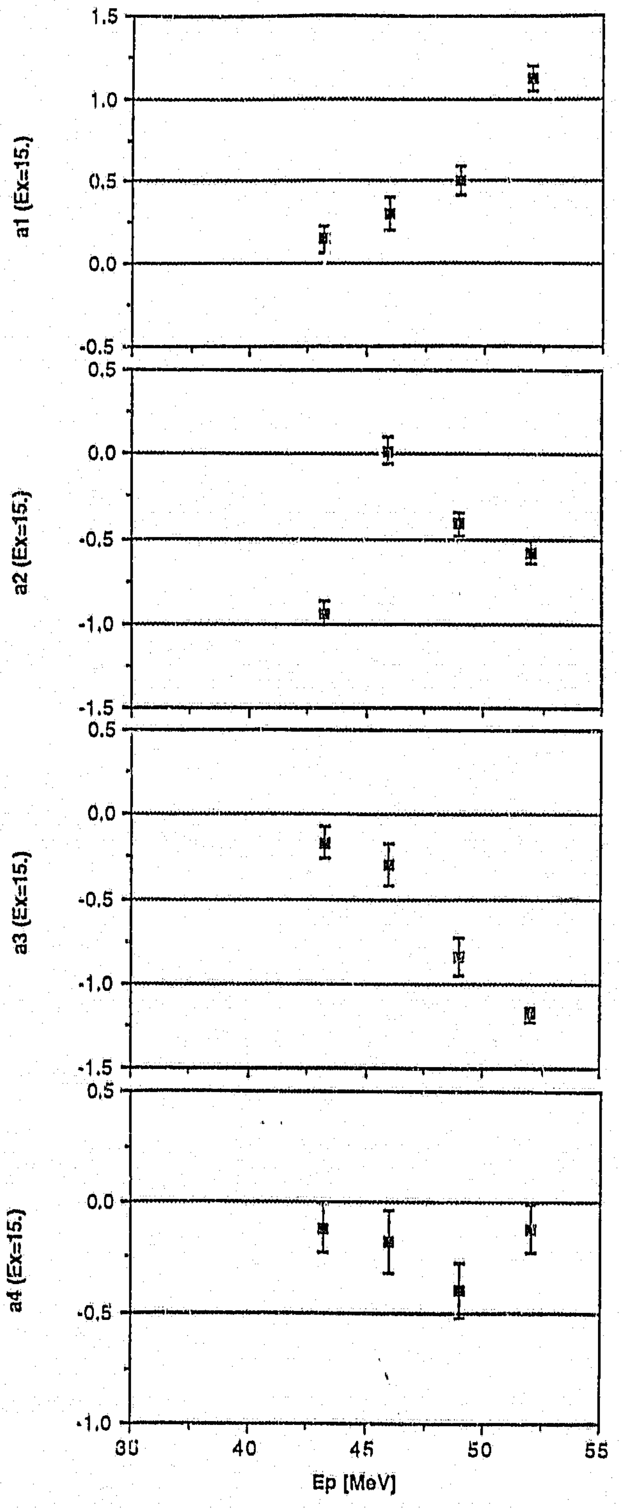

FIGURE 25 Legendre polynomial coefficients as a function of proton energy for the reaction $^{12}C(p,\gamma_x)^{13}N^*$ at $[E_x = 15. MeV]$.

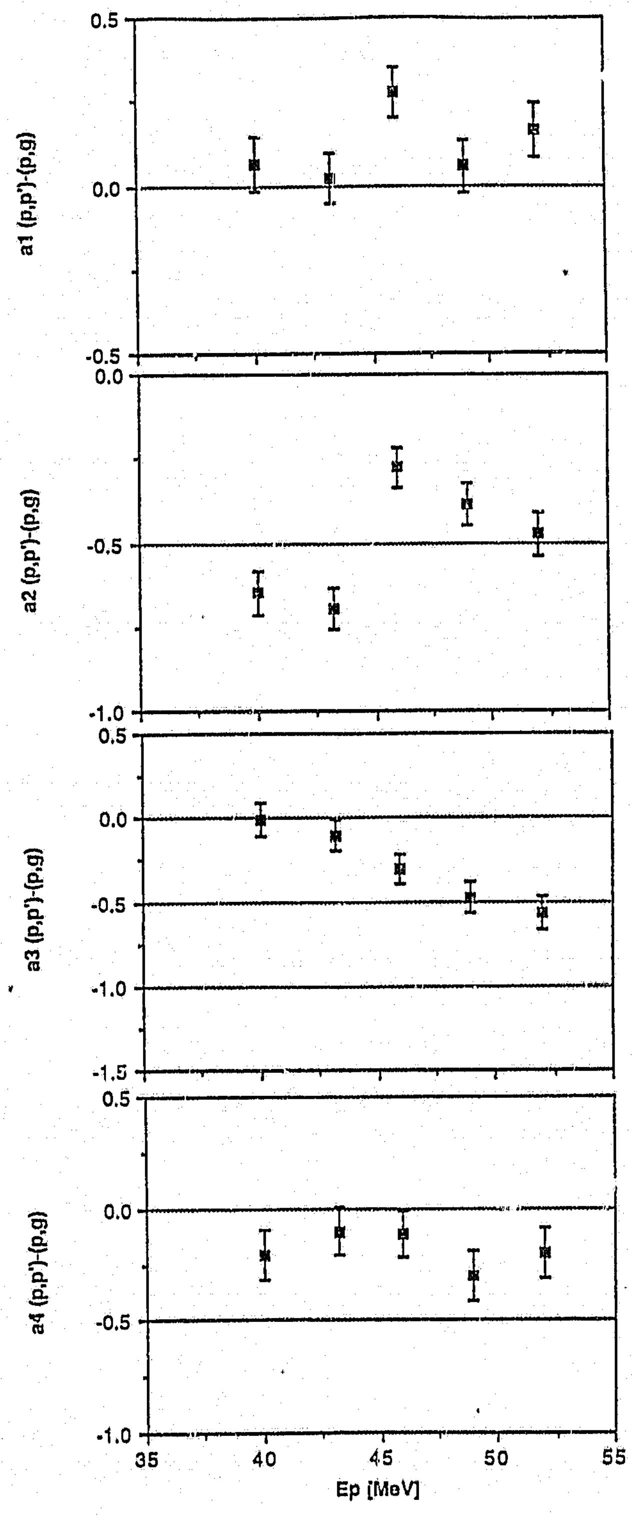

FIGURE 26 Legendre polynomial coefficients as a function of proton energy for the reaction $^{12}C(p,p'\gamma)^{12}C^*$ superimposed on competing $^{12}C(p,\gamma_x)^{13}N^*$ transitions.

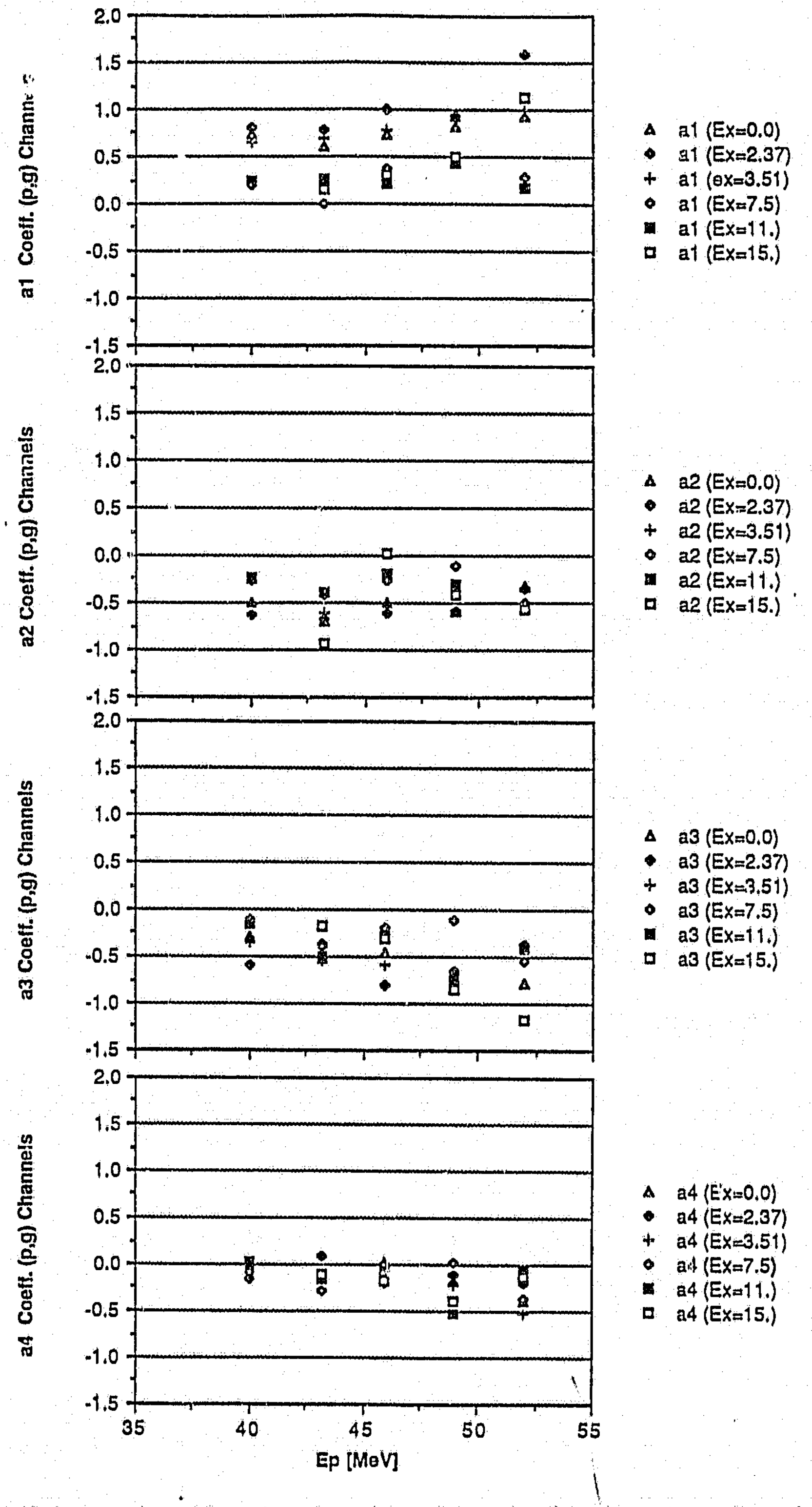

FIGURE 27 A comparison of Legendre polynomial coefficients for all (p,γ) transitions. Errors have been removed for better reading.

compound nuclei formed by proton radiative capture that in these two nuclei the behaviour of the a_i coefficients was well reproduced by two calculations [23] [24], that were based on substantially similar interaction models. A direct single proton transition amplitude was assumed to interfere with a semidirect term through the intermediate excitation of the GDR and GQR resonances. The very good agreement of data and theory over a large energy range showed that the rather sharp change of slope in the a_3 and a_4 coefficients around $E_x = 45\,\text{MeV}$ both in ^{12}C and ^{16}O is due to a rapid increase in quadrupole strength that the theory correctly predicts. Moreover the (γ, p_0) angular coefficients require, to be reproduced, some octupole strength above $E_x = 60\,\text{MeV}$. It should be noticed that the for both ^{12}C and ^{16}O the electric dipole and the electric quadrupole RPA cross sections [24] are extended over a range of 80-100 MeV with the E2 decreasing much more slowly than for the E1 above the region of the $2\hbar\omega$ excitation. Although a RPA calculation for ^{13}N would be extremely difficult one can extend the findings on the two doubly closed shell nuclei to ^{13}N at least in a qualitative way. This has in fact been done to interpret proton radiative capture to ^{13}N at $E_x < 42\,\text{MeV}$. The total cross section shows a smooth tail above the GDR, the angular distributions show a strong E1 component and dipole-quadrupole interference becoming relevant when the a_3 coefficient changes slope i.e. above $E_x = 28\,\text{MeV}$ to resettle at an average constant value of about -0.5 above $E_x = 35\,\text{MeV}$. The extension that we made to excitation energies as high as 50 MeV matches remarkably well this picture (see figures 20 and 21). The $\frac{1}{2}^-$ g.s. and the $\frac{3}{2}^-$ 3.51 MeV states are members of the same rotational band, therefore one expects in principle to find similar configurations for collective excitations built on each of the two states and consequently one would expect similar Legendre polynomial coefficients to be found. This is indeed the case. Our (p, γ_0) and (p, γ_{2+3}) a_1 coefficients show a marked increase from about 0.7 at $E_x = 39\,\text{MeV}$ to about 1.0 at $E_x = 50\,\text{MeV}$. This is accompained by a similar trend in a_2 with values increasing from -0.6 to 0.25, by a_3 values scattered around -0.5 and by a_4 coefficients that start departing from zero only above 50 MeV. The large absolute values of a_1 and a_2 are evidence of very strong interferences between the dipole and quadrupole mode. Interpreting the coefficients to first order leads us to assume that both E1 (increase of a_2) and E2 (increase in a_4) are increasing and at the same time their interference. This cannot be reconciled with the distributions of RPA quadrupole and dipole strength given in ^{12}C and ^{16}O. Both ^{12}C and ^{16}O have an E1 component which is roughly constant or slowly decreasing around 40-50 MeV but with more structure present in E2, which (according to the experimental findings . . in ^{16}O) should be shifted 5-6 MeV upwards with respect to the theoretical estimates that locate the peak of the isovector component at 38 MeV. Therefore one considers a more complex mechanism such as the interference at these energies of the $1\hbar\omega$ GDR, the $2\hbar\omega$ GDR and a broad quadrupole excitation. As remarked before, the a_5 coefficient is due in first order to (E2,E3) interference, being equal to zero does not indicate the presence of octupole excitation. A limit to any interpretation of proton radiative capture to the g.s and the 3.51 MeV state at present, is that the only theoretical calculation available [25] for ^{13}N is an evaluation of quadrupole strength above 20 MeV using a phenomenological semidirect model [26] [27], which is still under completion.

We can consider also other excited final states in ^{13}N, on the basis of the complete set of data collected. Again we observe that the 2.37 MeV ($\frac{1}{2}^+$), the 6.88 MeV($\frac{3}{2}^+$) or the 7.88 MeV($\frac{3}{2}^+$) states could be members of the same rotational band and have therefore a similar configuration and show similar a_i coefficients. Within the uncertainties in the extraction of Legendre coefficients, for weak transitions as are those to highly excited states, and with the possibility that kinematic factors could enhance the coefficients with respect to those of other members of the same rotational band, this seems the case. The interpretation of the a_i coefficients for these secondary transition channels in terms of interfering E1 and E2 modes is obviously much more difficult that in the previous case. On qualitative grounds one could observe that there is not evidence of the large E1 E2 interference that produced remarkable variations of the a_i coefficients in the energy range explored for the two major transitions. On the countrary, with maybe the exception of the states around 15 MeV, the a_i coefficients display an almost constant trend.

When we are in the presence of a large superposition of $(p,p'\gamma)$ and (p,γ) transitions, the angular distributions are affected, as is clear from the way they are distorted in figure 17. The (p,p') channel should be due basically to the E1 mode since it involves a $\Delta J^\pi = 1^-$ difference and as a matter of fact the angular distribution peaks move towards the 90 deg mark quite noticeably for energies like 40 and 43.2 MeV where the $2\hbar\omega$ excitation should not be at its peak. To be noted also is that a_1 could well be compatible with zero as we look at figure 26, and a_2 could well be compatible with -0.5, if we could separate the two contributions in the gamma spectra.

The second point to establish is the mechanism of excitation of these dominantly dipole transitions. This can be extracted from previous experience in different nuclei and from the detailed analysis of our excitation functions. It has been shown repeatedly that in proton radiative capture, strong transitions can be due to the building of a dipole excitation upon any of the nuclear excited states that have a large parentage with a configuration in which an inert core is coupled to a single particle in a shell model orbit. Giant resonances are observed in many such exit channels, as remarked in chapter 1, and this picture holds for every nucleus so far investigated. A remarkable feature of the general overview presently available is the build up of such a dipole mode even upon the g.s. GDR to produce a second harmonic GDR. This phenomenon has been clearly and extensively investigated for ^{12}C. Our data show, with respect to previous analyses of the $^{12}C(p,\gamma)^{13}N$, based on a single energy point [4], that the phenomena observed are complex and that the extraction of second harmonic GDR cross sections in ^{13}N is only possible above $E_p > 50\,\text{MeV}$. If we look at the excitation functions of figure 28, secondary resonances are observed in some of the possible reaction channels just around $E_x \approx 45\,\text{MeV}$, i.e. at an excitation energy roughly corresponding to that of the expected $2\hbar\omega$ collective mode. We see a resonance $8-9\,\text{MeV}$ wide in the γ_0 channel and about 10 MeV wide in the γ_{2+3} channel, and an off-statistics increase of the excitation function in the transition to the pair of states at $6.88\,\text{MeV}(\frac{3}{2}^+)$ and $7.90\,\text{MeV}(\frac{3}{2}^+)$. The strength that builds up in photon spectra to final states around $E_x = 22\,\text{MeV}$, as seen at $E_p = 52$ and $E_p = 54\,\text{MeV}$, could constitute direct evidence of a $2\hbar\omega$ collective excitation, if we could identify these final states as the major 2p-1h components of the GDR built upon the $\frac{1}{2}^-$ ^{13}N g.s. and if we could separate the (p,γ) and the $(p,p'\gamma)$ excitation functions already from 43 MeV to properly follow the excitation curve for this reaction channel. No random phase approximation (RPA) calculation has been made for ^{13}N for the spread of the dipole strength over 2p-1h states at excitation energies around 20 MeV so the identification of the final states involved in this particular reaction channel cannot be more precise than that done on the basis of our

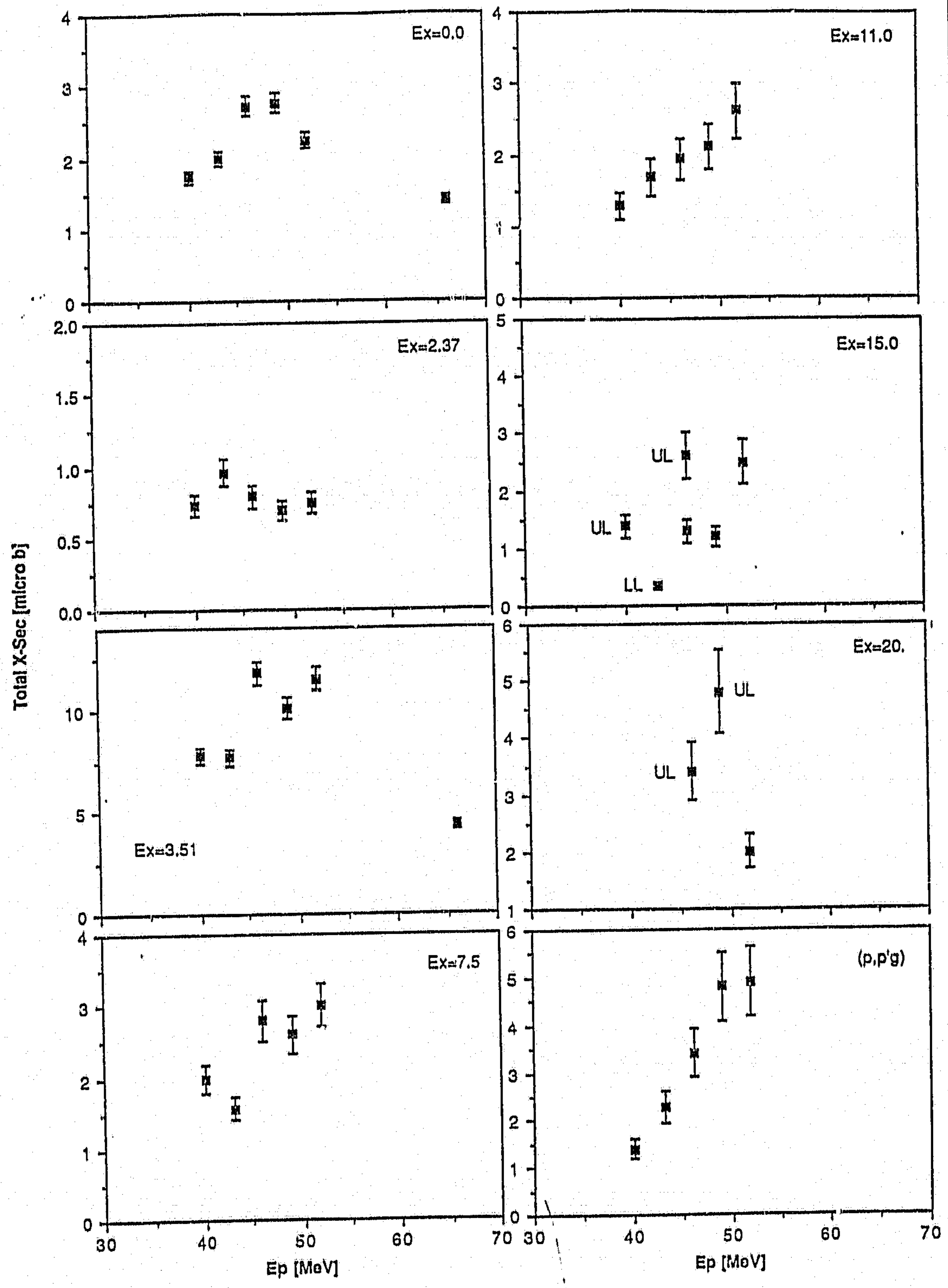

FIGURE 28 A summary of total cross sections, extracte... m the integration of our fitted angular distributions. Upper limits (UL) or lower limits (LL) are indicated.

energy calibration li: e and on the assignment of positive parity and momentum of 1/2 or 3/2 that is imposed by the ground state momentum sum with a dipole photon $J^\pi = 1^-$. The $2\hbar\omega$ excitation has therefore to be based on negative parity states at excitation energies around 44 MeV and angular momenta between 1/2 and 5/2. What we are observing as secondary resonances in the excitation function of (p,γ) capture to low lying states in ^{13}N is coupling by electromagnetic deexcitation of these $E_x \approx 44$ MeV states to the g.s., the 3.51-3.54 MeV pair, and possibly the 6.88-7.90 pair. At these resonances the angular coefficients depart substantially from the smooth trend that is consistently observed from $E_x = 30$ MeV onwards [4], and absolute cross sections are much higher than for any other transition. This would mean that the $2\hbar\omega \rightarrow 1\hbar\omega$ transition is depleted by kinematical factors since the upper limit for this transition attributed from the $(p,p') + (p,\gamma)$ cross sections is at 46 and 49 MeV of the order of 5 μb against 2.6 μb in the (p,γ_0) channel and 11 μb in the (p,γ_{2+3}) channel.

REFERENCES FOR CHAPTER 4

1) S.Hanna
Lect. Notes in Phys. 61(1977)275

2) P.E.Hodgson
Nuclear reactions and nuclear structure Clarendon Press 1971

3) K.A.Snover
Ann. Rev. Nucl. Part. Sci. 36(1986)545

4) M.Anghinolfi, P.Corvisiero M.Guarnone, G.Ricco, M.Sanzone, M.Taiuti and A.Zucchiatti
Persp. in Nucl. Phys. at Int. En. World Scient 1983 pg 160

5) P.S.Fisher, D.F.Measday, F.A.Nikolaev, A.Kalimkov and B.Clegg
Nucl. Phys. 45(1963)113

6) S.L.Blatt, H.J.Hausman, L.G.Arnold, R.G.Seyler, R.N.Boyd, T.R.Donoghue, P.Koncz, M.A.Kovash, A.D. Bacher and C.C.Foster
Phys. Rev. C30(1984)423

7) T.Shibata, T.Satoh, K.Kamikubota, Y.Nagai and H.Ejiri
RCNP Ann. Rep. 1986 pg. 125

8) M.Anghinolfi, P.Corvisiero, G.Ricco, M.Taiuti and A.Zucchiatti
Nucl. Phys. A399(1983)66

9) P.Corvisiero
Private Communication

10) M.Anghinolfi, P.Corvisiero, E.Durante, M.Guarnone, M.Taiuti and A.Zucchiatti
Il Nuovo Cim. 77A(1983)277

11) S.L.Blatt
AIP Conf. Proc. 125(1985)pg 570

12) D.H.Dowell
AIP Conf. Proc. 125(1985)pg 597

13) H.Ejiri, T.Shibata, Y.Nagai, T.Kishimoto, H.Ohsuni, N.Kamikubota and T.Satoh
AIP Conf. Proc. 125(1985)pg 582

14) P.Corvisiero, M.Taiuti, A.Zucchiatti and M.Anghinolfi
Nucl. Instr. and Meth. 185(1981)291

15) D.H.Dowell, W.P.Ziegler, A.M.Sandorfi, B.Ziegler and B.Schoch
Nucl. Instr. and Meth. A254(1987)570

16) D.R.Chakrabarty, S.Sen, M.Thoennessen, N.Alamanos, P.Paul, R.Schicker, J.Satchel and J.J.Gaardhoje
Phys. Rev. C36(1987)1886

17) R.Whitton
Work. on Rad. Capt. Sigtuna 1987 pg 271

18) M.T.Collins, A.M.Sandorfi, D.H.Hoffmann and M.K.Salomaa
Phys. Rev. Lett. 49(1982)1553

19) P.Buenerd, P.Martin, P.De Santignon and J.M.Loiseaux
Nucl. Phys. A286(1977)377

20) P.Corvisiero
Private Communication

21) G.Kernel, W.A.Mason and N.W.Tanner
Nucl. Instr. and Meth. 89(1970)1

22) S.Ferroni, G.Ricco, G.A.Rottigni, M.Sanzone and G.Lo Bianco
Il Nuovo Cim. 35A(1976)15

23) M.Gary and H.Hebach
Phys. Rep. 1(1981)1

24) M.Cavinato, M.Marangoni, P.Ottaviani and A.M.Saruis
Nucl. Phys. A273(1982)445

25) P.Corvisiero and M.M.Giannini
Private Communication (1988)

26) M.M.Giannini and G.Ricco
Ann. of Phys. 102(1976)458

27) M.M.Giannini, G.Ricco and A.Zucchiatti
Ann. of Phys. 124(1980)208

CHAPTER 5

OVERALL SUMMARY AND DISCUSSION

The objectives of this thesis were many and specific, being an essential part of the program of the Wits-CSIR Schonland Research Centre for Nuclear Sciences to develop a line of research based upon the experimental facilities of the National Accelerator Centre at Faure and projected towards medium energy nuclear physics. I would like to summarize the basic points.

a) The first objective was the design of a medium energy gamma-ray spectrometer, with energy resolution of the order of 2% from 20 to 50 MeV, detection efficiency better than 20% in typical experimental conditions coupled to a flexible electronics system to ensure complete digital and analog analysis of reaction parameters. The aim of the project was to establish and extend photon detection facilities at NAC, already provided with a low energy gamma correlation table, by a versatile medium-energy gamma-ray spectrometer, with excellent performance so to provide a window to a medium energy research program as, for instance, proton radiative capture, neutron capture at and above threshold, and particle-gamma correlations.

b) The detector development has been founded largely on a numerical simulation technique based upon a Monte Carlo code that includes all physical processes involved in the conversion of the electromagnetic shower energy, with emphasis given to a specific way of treating the bremsstrahlung energy losses and to the positron annihilation both in-flight and at rest. The Monte Carlo technique has proved a reliable and flexible tool to investigate thoroughly the dependance of resolution and efficiency on the geometrical parameters of the detector, and has led rapidly to the completion of the project.

c) The results of our simulation studies and of technological improvements, specifically intended to enhance the performance of scintillation detectors of this type, have been utilized by Bicron Corporation to produce a large volume sodium iodide crystal and a sector divided plastic scintillation anticoincidence shroud, that in laboratory tests showed that they met the design expectations, both in uniformity and in energy resolution at radioactive source gamma-ray energies.

d) Extensive specific investigations have been carried out at the SRCNS where a 7 MeV proton beam from the Tandem accelerator was captured in a thin ^{11}B target to produce gamma-rays of energy around 22 MeV. All critical experimental parameters, such as beam current, target thickness, detector uniformity, plastic scintillator rejection threshold, electronics stability, have been finely optimized to prove that the design expectations were effectively fulfilled by the spectrometer. The excellent performance has been *de facto* maintained at NAC where typical experimental conditions included thick targets, high beam currents, large neutron background, lower capture cross section with consequent longer acquisition times. A flexible electronics system has allowed clear separation of gamma events, good rejection of spurious (pile-up) events and thorough investigation of any aspect of the process investigated.

e) The first experimental program carried out after the detector wasset up has concerned an extensive study of proton radiative capture to ^{13}N with data collected at proton energies from 40 to 66 MeV, with complete angular distribution measurements at each energy point. The aim was to investigate the mechanism of transitions to the ground and excited states of ^{13}N in the region of the $2\hbar\omega$ second harmonic of the g.s. GDR. Indeed we have accumulated, during this work, the most complete and accurate set of data for this nucleus in this energy region. The picture that emerges from our results is rather new with respect to previous lower energy analyses, in many aspects. The strong transitions to the ground and to the second excited state, are both characterised by strong dipole-quadrupole interference possibly by the interference of three resonances. In both channels a broad resonance is seen at these energies, due to the direct coupling of the $2\hbar\omega$ collective excitation to low-lying ^{13}N states. The behaviour of the angular coefficients is essentially equivalent in the two cases, proving that the internal structure of the two states, both part of the same rotational band, is effectively similar. We have demonstrated that radiative decay to states in the g.s. GDR region cannot be uniquely identified in the gamma spectra, since it is largely superimposed upon inelastic proton scattering from ^{12}C. Only at very high energies

($E_p > 52\,\text{MeV}$), do the fixed energy inelastic scattering gammas and the kinematically defined capture gammas become clearly distinguished, but we should then be far from the actual resonant point of the capture channel. The effect of the $2\hbar\omega$ collective excitation is nevertheless evident in the transition to low-lying ^{13}N states. Similarly complete results have been obtained for several excited states up to $E_x \approx 15\,\text{MeV}$. There the extraction of cross sections is affected by the increasing background, but even within the limitations imposed by larger experimental errors, some general features can be understood, as for example the similarity of Legendre coefficients for states that should be members of the same rotational band and therefore have similar structure.

f) Our ambitions were of course to be able to give a more complete theoretical interpretation to account for the observations we made and in this we are definitely constrained since the theoretical treatment is not yet up to the experimental measurements and represents the next generation of research in this regard.